

The hydrogen-air burning rate near the lean flammability limit

D. Fernández-Galisteo^{1,*}, A.L. Sánchez¹, A. Liñán², F.A. Williams³

¹ Dept. Ingeniería Térmica y de Fluidos, Universidad Carlos III de Madrid, Spain

² ETSI Aeronáuticos, Universidad Politécnica de Madrid, Spain

³ Dept. of Mechanical and Aerospace Engineering, University of California San Diego, USA

Abstract

This paper investigates the inner structure of the thin reactive layer of hydrogen-air fuel-lean deflagrations close to the flammability limit. The analysis, which employs seven elementary reactions for the chemistry description, uses the ratio of the characteristic radical and fuel concentrations as a small asymptotic parameter, enabling an accurate analytic expression for the resulting burning rate. The analysis reveals that the steady-state assumption for chemical intermediaries, applicable on the hot side of the reactive layer, fails however as the crossover temperature is approached, providing a nonnegligible higher-order correction to the burning rate. The results can be useful, for instance, in future investigations of hydrogen deflagration instabilities near the lean flammability limit.

Introduction

Theoretical investigations of flame dynamics often take into account that the inner structure of planar steady deflagrations typically shows a two-layer structure including a frozen upstream preheat region and a much thinner diffusive-reactive layer with negligible convection. When considering flame perturbations, unsteady effects, as well as curvature and strain effects, enter first to modify the thicker preheat region, whereas the reactive-diffusive layer remains planar in the first approximation, and reacts to the external perturbation in a quasi-steady manner, giving a burning rate (fuel burnt per unit flame surface) that is mainly a function of the perturbed burnt temperature. This paper is intended to facilitate these analyses by providing a simplified description for the resulting burning rate in the case of hydrogen-air flames near the lean flammability limit, to be used for instance in the investigation of diffusive-thermal instabilities leading to cellular structures in such flames.

The present work builds on our previous investigation [1], which identified a detailed mechanism of seven elementary reactions, shown below in Table 1, that describes accurately the propagation of atmospheric and sub-atmospheric lean hydrogen-air flames. The resulting chemistry description predicts, in particular, a kinetically-controlled flammability limit at which the planar deflagration velocity vanishes, when the adiabatic flame temperature equals the crossover temperature, the latter defined such that the rate of reaction $\text{H} + \text{O}_2 \xrightarrow{1f} \text{OH} + \text{O}$ equals that of reaction $\text{H} + \text{O}_2 + \text{M} \xrightarrow{4f} \text{HO}_2 + \text{M}$. It also predicts that all chemical intermediaries appear in the thin reaction layer in concentrations that are much smaller than that of the fuel, and can be consequently computed in the steady-state approximation. The development leads to a one-step reduced mechanism in which the main species react according to the single overall reaction $2\text{H}_2 + \text{O}_2 \rightarrow 2\text{H}_2\text{O}$ with a non-Arrhenius global rate. The resulting steady-state expressions for H, O and OH predict radicals to exist only in a small intermediate temperature range that

extends from crossover to the burnt temperature. Radical concentrations disappear abruptly at crossover where the steady-state assumption fail and the resulting radical profiles show an unrealistic discontinuous slope.

The analysis below will address the structure of the thin reactive-diffusive layer in lean hydrogen-air deflagrations, including the region where steady-state approximations hold for all radicals and the layer of steady-state failure, located around the crossover temperature. The ratio, ε , of the characteristic values of the H-atom and H_2 concentrations in the reaction layer, a small quantity for lean flames near the flammability limit, will be identified as the relevant asymptotic parameter in the development.

Specific objectives and problem formulation

As shown recently [1], for hydrogen-air mixtures that are very fuel lean, the seven steps shown in Table 1 suffice to describe accurately flame propagation velocity. The table shows the rate constants for all reactions, taken from the so-called San Diego mechanism [2], which has been tested to give excellent results when applied to the description of hydrogen combustion [3].

Reaction	A^a	n	$T_a[\text{K}]$
1. $\text{H} + \text{O}_2 \rightleftharpoons \text{OH} + \text{O}$	3.52×10^{16}	-0.7	8590
2. $\text{H}_2 + \text{O} \rightleftharpoons \text{OH} + \text{H}$	5.06×10^4	2.67	3166
3. $\text{H}_2 + \text{OH} \rightleftharpoons \text{H}_2\text{O} + \text{H}$	1.17×10^9	1.3	1829
4f. $\text{H} + \text{O}_2 + \text{M} \rightarrow \text{HO}_2 + \text{M}^b$	k_0	-1.4	0
	k_∞	0.44	0
5f. $\text{HO}_2 + \text{H} \rightarrow \text{OH} + \text{OH}$	7.08×10^{13}	0	148
6f. $\text{HO}_2 + \text{H} \rightarrow \text{H}_2 + \text{O}_2$	1.66×10^{13}	0	414
7f. $\text{HO}_2 + \text{OH} \rightarrow \text{H}_2\text{O} + \text{O}_2$	2.89×10^{13}	0	-250

^aUnits are mol, s, cm³, and K.

^bChaperon efficiencies are 2.5 for H_2 , 16.0 for H_2O , and 1.0 for all other species; Troe falloff with $F_c = 0.5$ [5].

Table 1: The 7-step mechanism with rate coefficients in the Arrhenius form $k = AT^n \exp(-T_a/T)$ as given in [3].

A sample computation of a steady planar deflagration obtained with the COSILAB code [4] with this 7-step mechanism is shown in Fig. 1 for pressure $p = 1$ atm, initial temperature $T_u = 300$ K and equivalence ratio

*Corresponding author: galisteo@ing.uc3m.es
Proceedings of the European Combustion Meeting 2009

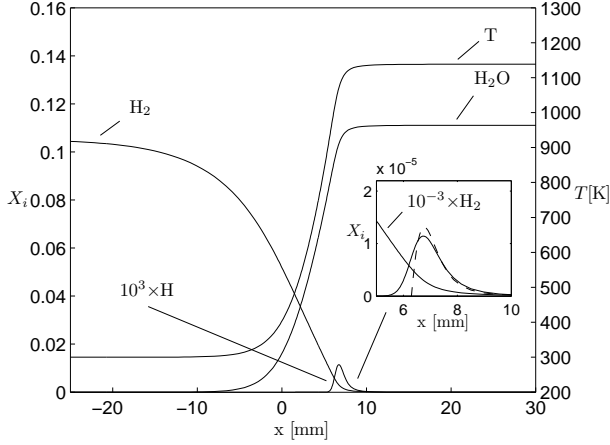


Figure 1: The temperature and mole fractions across a pre-mixed hydrogen-air mixture for $p = 1$ atm, $T_u = 300$ K and $\phi = 0.28$ as calculated with the 7-step short mechanism. The inset compares the H-atom mole fraction computed numerically with that predicted by the steady-state expression (29).

$\phi = 0.28$. As can be seen, for these very lean conditions radicals only exist in a relatively thin reactive layer, that is preceded by a chemically frozen preheat region. The main effect of curvature and unsteadiness, together with preferential diffusion effects, is to change the structure of the preheat region from that shown in the figure for a steady planar flame, modifying the resulting burnt temperature which mainly manages the associated burning rate.

We shall investigate below the structure of the thin reactive layer where radicals are present to determine the fuel mass burning rate as a function of the burnt temperature, giving results that may be used not only for computations of steady planar deflagration velocities but also in studies of flame dynamics and stability. Because of its small thickness, convection can be neglected in the first approximation in this reactive layer, along with changes of density ρ and thermal diffusivity D_T from their downstream values at equilibrium. If n is defined as the coordinate normal to the reaction layer, then the resulting species conservation equations become

$$-\frac{D_T}{L_{H_2}} \frac{d^2 C_{H_2}}{dn^2} = -\omega_2 - \omega_3 + \omega_{6f} \quad (1)$$

$$-\frac{D_T}{L_{O_2}} \frac{d^2 C_{O_2}}{dn^2} = -\omega_1 - \omega_{4f} + \omega_{6f} + \omega_{7f} \quad (2)$$

$$-\frac{D_T}{L_{H_2O}} \frac{d^2 C_{H_2O}}{dn^2} = \omega_3 + \omega_{7f}, \quad (3)$$

$$-\frac{D_T}{L_O} \frac{d^2 C_O}{dn^2} = \omega_1 - \omega_2 \quad (4)$$

$$-\frac{D_T}{L_{OH}} \frac{d^2 C_{OH}}{dn^2} = \omega_1 + \omega_2 - \omega_3 + 2\omega_{5f} - \omega_{7f} \quad (5)$$

$$-\frac{D_T}{L_H} \frac{d^2 C_H}{dn^2} = -\omega_1 + \omega_2 + \omega_3 - \omega_{4f} - \omega_{5f} - \omega_{6f} \quad (6)$$

$$-\frac{D_T}{L_{HO_2}} \frac{d^2 C_{HO_2}}{dn^2} = \omega_{4f} - \omega_{5f} - \omega_{6f} - \omega_{7f} \quad (7)$$

where C_i and L_i are the concentration and Lewis number of species i . At the same level of approximation, the energy conservation equation becomes

$$\rho c_p D_T \frac{d^2 T}{dn^2} = \sum h_i^o \dot{C}_i, \quad (8)$$

where c_p is the specific heat at constant pressure, assumed to be constant, T is the temperature, h_i^o is the enthalpy of formation per mol of species i , and \dot{C}_i denotes its corresponding chemical production rate (moles per unit volume per unit time), to be computed from the rates ω_j of the elementary reactions shown in Table 1. The above equations are to be integrated with boundary conditions corresponding to matching with the upstream chemically frozen preheat region as $n \rightarrow -\infty$

$$\begin{aligned} \frac{\dot{m}_{H_2}}{W_{H_2} D_T} &= -\frac{1}{L_{H_2}} \frac{dC_{H_2}}{dn} = -\frac{2}{L_{O_2}} \frac{dC_{O_2}}{dn} \\ &= \frac{1}{L_{H_2O}} \frac{dC_{H_2O}}{dn} = -\frac{\rho c_p}{h_{H_2O}^o} \frac{dT}{dn} \end{aligned} \quad (9)$$

and

$$C_O = C_{OH} = C_H = C_{HO_2} = 0, \quad (10)$$

where \dot{m}_{H_2} is the mass fuel burning rate and W_{H_2} is the molecular mass of H_2 . The accompanying boundary conditions as $n \rightarrow +\infty$ correspond to the downstream equilibrium state

$$\begin{aligned} C_{H_2} &= C_{O_2} - C_{O_{2\infty}} = C_{H_2O} - C_{H_2O_{\infty}} \\ &= C_O = C_{OH} = C_H = C_{HO_2} = 0, \end{aligned} \quad (11)$$

where the subscript ∞ denotes the burnt equilibrium state.

The solution of the above problem for given values of T_∞ , $C_{O_{2\infty}}$, $C_{H_2O_{\infty}}$ and pressure determines the fuel burning rate \dot{m}_{H_2} . To facilitate the development, it is convenient to combine linearly (1), (2) and (3) with (4)–(7) to obtain the alternative equations

$$D_T \frac{d^2}{dn^2} \left(\frac{C_{H_2}}{L_{H_2}} + \frac{C_O}{L_O} + \frac{1}{2} \frac{C_{OH}}{L_{OH}} + \frac{3}{2} \frac{C_H}{L_H} - \frac{1}{2} \frac{C_{HO_2}}{L_{HO_2}} \right) = 2\omega_{4f} \quad (12)$$

$$D_T \frac{d^2}{dn^2} \left(\frac{C_{O_2}}{L_{O_2}} + \frac{C_O}{L_O} + \frac{1}{2} \frac{C_{OH}}{L_{OH}} + \frac{1}{2} \frac{C_H}{L_H} + \frac{1}{2} \frac{C_{HO_2}}{L_{HO_2}} \right) = \omega_{4f} \quad (13)$$

$$D_T \frac{d^2}{dn^2} \left(\frac{C_{H_2O}}{L_{H_2O}} - \frac{C_O}{L_O} - \frac{C_H}{L_H} + \frac{C_{HO_2}}{L_{HO_2}} \right) = -2\omega_{4f}, \quad (14)$$

where

$$\omega_{4f} = k_{4f} C_M C_{O_2} C_H \quad (15)$$

is the rate of the three-body recombination reaction, with

$$C_M = p/(R^o T) + 15C_{H_2O} + C_{H_2}, \quad (16)$$

representing the effective third-body concentration, which accounts for the non-unity third-body Chaperon efficiencies of water vapor and molecular hydrogen. Integrating

once (12) with the boundary conditions given above provides

$$\dot{m}_{H_2} = 2W_{H_2} \int_{-\infty}^{+\infty} k_{4f} C_M C_{O_2} C_H dn, \quad (17)$$

indicating that the burning rate is linearly proportional to rate of the recombination reaction $4f$ integrated across the flame. An accurate description of the H-atom concentration is therefore needed to compute \dot{m}_{H_2} . We shall see below that such a description requires consideration of two different regions: a relatively thick layer where all radicals follow a steady-state approximation and a thinner upstream layer where the steady-state solutions for O, OH and H break down. Both regions will be analyzed separately below.

Fuel burning rate in the steady-state region

As seen in Fig. 1 for the radical H, taken as representative of the radical pool, near the lean flammability limit radicals appear in concentrations that are much smaller than those of H_2 . Neglecting radical concentrations on the left-hand side of (12), (13) and (14) provides

$$\frac{D_T}{L_{O_2}} \frac{d^2 C_{O_2}}{dn^2} = -\frac{D_T}{2L_{H_2O}} \frac{d^2 C_{H_2O}}{dn^2} = \frac{D_T}{2L_{H_2}} \frac{d^2 C_{H_2}}{dn^2} = \omega_{4f}, \quad (18)$$

indicating that, in the first approximation, the fuel burns as dictated by the irreversible overall reaction $2H_2 + O_2 \rightarrow 2H_2O$ with a rate equal to that of reaction $4f$. At the same level of approximation, the energy conservation equation becomes

$$\rho c_p D_T \frac{d^2 T}{dn^2} = -2q\omega_{4f}, \quad (19)$$

and diffusive transport of radicals can be neglected in (4)–(7) to give

$$\omega_1 - \omega_2 = 0 \quad (20)$$

$$\omega_1 + \omega_2 - \omega_3 + 2\omega_{5f} - \omega_{7f} = 0 \quad (21)$$

$$-\omega_1 + \omega_2 + \omega_3 - \omega_{4f} - \omega_{5f} - \omega_{6f} = 0 \quad (22)$$

$$\omega_{4f} - \omega_{5f} - \omega_{6f} - \omega_{7f} = 0. \quad (23)$$

In (19), $q = -h_{H_2O}^o$ denotes the amount of heat released per mole of H_2 consumed. The new set of equations (18)–(23), including the steady-state approximations (20)–(23) for the radicals, apply at leading order provided the radicals concentrations are much smaller than C_{H_2} .

Using the boundary conditions as $n \rightarrow \infty$ in integrating the first two equations in (18) yields

$$C_{O_2} = C_{O_2\infty} + \frac{L_{O_2}}{2L_{H_2}} C_{H_2} \quad (24)$$

$$C_{H_2O} = C_{H_2O\infty} - \frac{L_{H_2O}}{L_{H_2}} C_{H_2} \quad (25)$$

while a similar integration obtained from a linear combination of the last equation in (18) and (19), gives

$$T_\infty - T = qC_{H_2}/(\rho c_p L_{H_2}). \quad (26)$$

Equations (24)–(26) can be used to relate the concentrations of oxygen and water vapor and the temperature to the local H_2 concentration. In the computations below, the values $L_{O_2} = 1.11$, $L_{H_2} = 0.3$, $L_{H_2O} = 0.83$ are employed for the different Lewis numbers, and the constant values of the density and specific heat are evaluated at equilibrium.

To proceed with the analysis, (20)–(23) must be solved to give expressions for the radical concentrations [1]. If the reverse reaction $2b$ is neglected, an excellent approximation under these fuel-lean conditions, the resulting explicit expressions become

$$C_{O_{ss}} = \frac{\alpha k_{3f} C_{H_2}}{G k_{1b}} \left(\frac{k_{1f}}{\alpha k_{4f} C_M} - 1 \right) \quad (27)$$

$$C_{OH_{ss}} = \frac{k_{2f} C_{H_2}}{k_{1b}} \left(\frac{k_{1f}}{\alpha k_{4f} C_M} - 1 \right) \quad (28)$$

$$C_{H_{ss}} = \frac{1}{G} \frac{k_{2f} k_{3f} C_{H_2}^2}{k_{1b} k_{4f} C_M C_{O_2}} \left(\frac{k_{1f}}{\alpha k_{4f} C_M} - 1 \right), \quad (29)$$

$$C_{HO_{2ss}} = \frac{k_{3f}}{(f + G)k_{7f}} C_{H_2}, \quad (30)$$

where

$$f = \frac{k_{5f} + k_{6f}}{k_{7f}} \frac{k_{3f}}{k_{4f} C_M} \frac{C_{H_2}}{C_{O_2}}, \quad (31)$$

$$G = \frac{1 + \gamma_{3b}}{2} + \frac{f}{2} \left\{ [1 + 2(3 + \gamma_{3b})/f + (1 + \gamma_{3b})^2/f^2]^{1/2} - 1 \right\} \quad (32)$$

and

$$\alpha = \frac{k_{6f} f / (k_{5f} + k_{6f}) + G}{f + G}, \quad (33)$$

with

$$\gamma_{3b} = \frac{k_{3b} C_{H_2O}}{k_{4f} C_M C_{O_2}}. \quad (34)$$

It is of interest that, according to (28), (29) and (27), in the steady-state approximation adopted here the concentrations of OH, H and O vanish as the temperature approaches the crossover value T_c , defined by the condition

$$k_{1f} = \alpha k_{4f} C_M, \quad (35)$$

giving a value that depends on the composition through the function α and the effective third-body concentration C_M . At temperatures below T_c the steady-state approximation predicts $C_O = C_{OH} = C_H = 0$, so that the reaction rate is cut off at that temperature. On the other hand, the concentration of the hydroperoxyl radical, given in (30), reaches however a nonzero value at the crossover temperature and is positive also for $T < T_c$.

To obtain the burning rate associated with the steady-state description the last equation in (18) multiplied by dC_{H_2}/dn may be integrated once with the boundary conditions as $n \rightarrow \pm\infty$ to give

$$(\dot{m}_{H_2})_{ss} = 2W_{H_2} \left(\frac{D_T}{L_{H_2}} \int_0^\infty \omega_{4f} dC_{H_2} \right)^{1/2}. \quad (36)$$

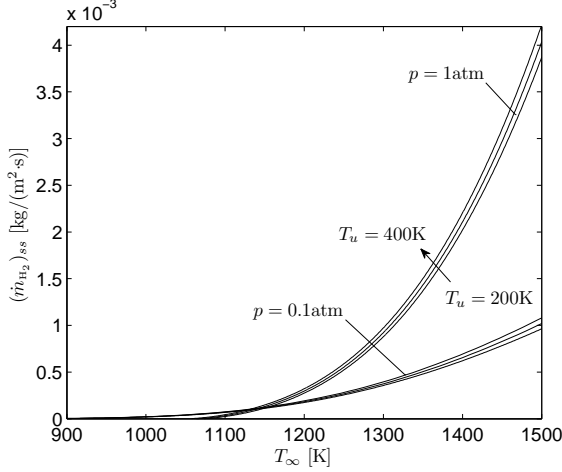


Figure 2: The variation of the fuel burning rate with the burnt temperature T_∞ for $p = 0.1$ atm and $p = 1$ atm; in the computation, for each T_∞ the values of $C_{O_2\infty}$ and $C_{H_2O\infty}$ are taken as the equilibrium values for a hydrogen-air planar deflagration with $T_u = (200, 300, 400)$ K.

Because of the reaction-rate cutoff at the crossover point, this expression becomes

$$(\dot{m}_{H_2})_{ss} = 2W_{H_2} \times \left(\frac{D_T}{L_{H_2}} \int_0^{C_{H_2c}} \frac{k_{2f}k_{3f}C_{H_2}^2}{Gk_{1b}} \left(\frac{k_{1f}}{\alpha k_{4f}C_M} - 1 \right) dC_{H_2} \right)^{1/2} \quad (37)$$

when the steady-state expression (29) is used to evaluate C_H . In the integration, use must be made of (26) to compute the temperature (and therefore evaluate the reaction-rate constants) in terms of C_{H_2} . Similarly, the concentrations C_{O_2} and C_{H_2O} , which enter in the computation of G , α and C_M , are to be evaluated from (24) and (25). The integration is extended until the H_2 concentration reaches its limiting value at crossover

$$C_{H_2c} = \rho c_p L_{H_2} (T_\infty - T_c) / q, \quad (38)$$

to be therefore determined as part of the integration.

The burning rate given in (37) depends mainly on the burnt temperature T_∞ , which appears in (26), and on the pressure, which determines C_M , whereas the dependence on the equilibrium composition through the values $C_{O_2\infty}$ and $C_{H_2O\infty}$ that enter in (24) and (25) is somewhat weaker. To investigate both dependences, the variation of $(\dot{m}_{H_2})_{ss}$ with T_∞ is shown in Fig.2 for $p = 0.1$ atm and $p = 1$ atm. In the computation, for each value of T_∞ , the accompanying values of $C_{O_2\infty}$ and $C_{H_2O\infty}$ are selected as the downstream equilibrium values of a planar deflagration with equivalence ratio ϕ such that the associated adiabatic flame temperature equals T_∞ . Clearly, for the deflagration considered, the relationship between ϕ and T_∞ depends on the value of the unburnt temperature T_u yielding therefore different values of $C_{O_2\infty}$ and $C_{H_2O\infty}$. However, these differences do not alter significantly the

resulting burning rate, as can be seen in Fig.2, indicating that $(\dot{m}_{H_2})_{ss}$ is mainly a function of T_∞ and p .

The crossover layer

The accuracy of the explicit steady-state expression (29) is demonstrated in the inset of Fig. 1, which includes the comparison of the H-atom profile determined numerically on the basis of the 7-step mechanism with that determined from evaluating (29). In the evaluation, use has been made of the profiles of reactant and water-vapor mol fractions and of temperature obtained numerically with the 7-step mechanism. It can be seen that the accuracy of the steady-state expression is excellent across the reaction layer, except at crossover, where the steady state predicts H atoms to disappear abruptly, thereby giving a profile with a discontinuous slope. Diffusive transport enters to remove this discontinuity, so that a smooth corner-layer profile replaces the abrupt change of the steady-state prediction when the 7-step mechanism is employed in the computations. Because of the direct proportionality of the burning rate and the H-atom content displayed in (17), the increased H-atom concentration in the layer of steady-state failure provides a nonnegligible additional contribution to the burning rate, which needs to be computed for increased accuracy.

Failure of the steady states for the radicals O, OH and H at a given upstream location is somewhat unexpected. To better clarify the problem it is of interest to write the radical conservation equations in dimensionless form, an effort that serves to identify the small parameter underlying the validity of the steady-state assumptions and the magnitude of the errors expected from the present analytical development. For that purpose, the fuel concentration is scaled with its crossover value C_{H_2c} according to $y_{H_2} = C_{H_2}/C_{H_2c}$, whereas the radical concentrations $y_O = C_O/C_{Oo}$, $y_{OH} = C_{OH}/C_{OHo}$ and $y_H = C_H/C_{Ho}$ are scaled with their characteristic values implied by (27)–(29)

$$C_{Oo} = \alpha \frac{k_{3f}C_{H_2c}}{Gk_{1b}} \quad (39)$$

$$C_{OHo} = \frac{k_{2f}C_{H_2c}}{k_{1b}} \quad (40)$$

$$C_{Ho} = \frac{1}{G} \frac{k_{2f}k_{3f}C_{H_2c}^2}{k_{1b}k_{4f}C_M C_{O_2c}}, \quad (41)$$

where the different reaction-rate constants are evaluated at the crossover temperature, which is also used in evaluating the effective third-body concentration C_M and the functions f and G from (16), (31), and (32), respectively, with the oxygen and water vapor concentrations evaluated from (24)–(25) at the H_2 concentration reaches crossover, that is from (38).

The characteristic thickness of the reaction region

$$\delta = [D_T / (k_{4f}C_M C_{O_2c} \varepsilon)]^{1/2}, \quad (42)$$

arising from an order-of-magnitude analysis of the last equation in (18), is employed to scale the dimensionless coordinate $x = n/\delta$, with

$$\varepsilon = \frac{C_{Ho}}{C_{H_2c}} = \frac{1}{G} \frac{k_{2f}k_{3f}C_{H_2c}}{k_{1b}k_{4f}C_M C_{O_2c}} \quad (43)$$

representing the characteristic H-to-H₂ concentration ratio, the small parameter for our steady-state analysis. Introducing these variables reduces (4)–(6) to the dimensionless form

$$-\varepsilon \frac{\Lambda_{\text{O}}}{L_{\text{O}}} \frac{d^2 y_{\text{O}}}{dx^2} = \frac{k_{1f}}{k_{4f} C_{\text{M}}} y_{\text{H}} - \alpha(y_{\text{OH}} y_{\text{O}} + y_{\text{H}_2} y_{\text{O}}) \quad (44)$$

$$-\varepsilon \frac{\Lambda_{\text{OH}}}{L_{\text{OH}}} \frac{d^2 y_{\text{OH}}}{dx^2} = \frac{k_{1f}}{k_{4f} C_{\text{M}}} y_{\text{H}} - \alpha(y_{\text{OH}} y_{\text{O}} - y_{\text{H}_2} y_{\text{O}}) - (2 + \gamma_{3b})(y_{\text{H}_2} y_{\text{OH}} - y_{\text{H}}) - 2\alpha y_{\text{H}} \quad (45)$$

$$-\varepsilon \frac{1}{L_{\text{H}}} \frac{d^2 y_{\text{H}}}{dx^2} = -\frac{k_{1f}}{k_{4f} C_{\text{M}}} y_{\text{H}} + \alpha(y_{\text{OH}} y_{\text{O}} + y_{\text{H}_2} y_{\text{O}}) + (2 + \gamma_{3b})(y_{\text{H}_2} y_{\text{OH}} - y_{\text{H}}) \quad (46)$$

where we have neglected the variation of C_{O_2} and $C_{\text{H}_2\text{O}}$ from their crossover values C_{O_2c} and $C_{\text{H}_2\text{O}c}$, along with the temperature dependence of the different reaction-rate constants, except that of reaction 1*f*, whose sensitivity near crossover must be taken into account. To achieve a more compact form, we have used the steady-state equation (7) to write $-\omega_{5f} - \omega_{6f} = -\omega_{4f} + \omega_{7f}$ in (6), and neglect the H₂ variation when writing ω_{5f} in (5). The constant radical-radical ratios $\Lambda_{\text{O}} = C_{\text{O}_\bullet}/C_{\text{H}_\bullet}$ and $\Lambda_{\text{OH}} = C_{\text{OH}_\bullet}/C_{\text{H}_\bullet}$ appear as factors of order unity. Since the hydroperoxyl steady-state approximation does not fail, one may use in the first approximation

$$C_{\text{HO}_2} = \frac{k_{3f}}{(f + G)k_{7f}} C_{\text{H}_2c} y_{\text{H}_2} \quad (47)$$

for the present purposes. The radical Lewis numbers $L_{\text{H}} = 0.18$, $L_{\text{O}} = 0.7$ and $L_{\text{OH}} = 0.73$ are used below in the numerical evaluations.

Equations (44)–(46) are the dimensionless form of (4)–(6). Although they are simplified by evaluating at crossover the O₂ and H₂O concentrations as well as all of the reaction-rate constants but k_{1f} , they still retain the essential nonlinearities of the problem, associated with consumption of fuel and with the temperature variation of the chain-branching controlling reaction 1*f*. One could in principle write similar conservation equations for y_{H_2} and T/T_c to provide the dimensionless formulation of the burning rate problem, to be solved by appropriately matching expansions of the different variables in powers of the asymptotically small parameter ε , but these additional equations are unnecessary for computing the H-atom concentration near crossover, and are therefore omitted here.

Due to their discontinuous gradients, the steady-state radical profiles do not constitute an acceptable solution at $x = 0$, because they would be associated with infinite values of the diffusive rates appearing on the left-hand sides of (44)–(46). In the solution that appears, radical diffusion becomes comparable to the chemical rates, yielding smooth profiles centered around $x = 0$ for the radicals, as seen for H in the 7-step computation shown in Fig. 1.

Failure of the steady-state approximation occurs at distances $x \sim \varepsilon^{1/3}$, where $y_{\text{O}} \sim y_{\text{OH}} \sim y_{\text{H}} \sim 1 - y_{\text{H}_2} \sim \varepsilon^{1/3}$ and $k_{1f}/(\alpha k_{4f} C_{\text{M}}) = 1 + Ax$, where

$$A = \frac{d}{dx} \left(\frac{k_{1f}}{\alpha k_{4f} C_{\text{M}}} \right) = \delta \frac{T_{1f}}{T_c^2} \left(\frac{dT}{dn} \right)_c, \quad (48)$$

as implied by a Taylor expansion near $x = 0$ with account taken of the temperature sensitivity of k_{1f} . The resulting factor A is of order $T_{1f}(T_\infty - T_c)/T_c^2$. Note that the temperature gradient in (48) can be related to the burning rate of the steady-state region through (9)

$$\left(\frac{dT}{dn} \right)_c = \frac{q}{\rho c_p} \frac{(\dot{m}_{\text{H}_2})_{ss}}{W_{\text{H}_2} D_T}. \quad (49)$$

Introducing into (44)–(46) expansions for the radicals of the form $y_{\text{O}} = \varepsilon^{1/3}(\varphi_{\text{O}}^0 + \varepsilon^{1/3}\varphi_{\text{O}}^1 \dots)$, $y_{\text{OH}} = \varepsilon^{1/3}(\varphi_{\text{OH}}^0 + \varepsilon^{1/3}\varphi_{\text{OH}}^1 \dots)$, and $y_{\text{H}} = \varepsilon^{1/3}(\varphi_{\text{H}}^0 + \varepsilon^{1/3}\varphi_{\text{H}}^1 \dots)$ yields at leading order the linear homogeneous problem

$$0 = \alpha(\varphi_{\text{H}}^0 - \varphi_{\text{O}}^0) \quad (50)$$

$$0 = -\alpha(\varphi_{\text{H}}^0 - \varphi_{\text{O}}^0) - (2 + \gamma_{3b})(\varphi_{\text{OH}}^0 - \varphi_{\text{H}}^0) \quad (51)$$

$$0 = -\alpha(\varphi_{\text{H}}^0 - \varphi_{\text{O}}^0) + (2 + \gamma_{3b})(\varphi_{\text{OH}}^0 - \varphi_{\text{H}}^0). \quad (52)$$

This problem has a nontrivial solution with

$$\varphi_{\text{O}}^0 = \varphi_{\text{OH}}^0 = \varphi_{\text{H}}^0 \quad (53)$$

because the determinant of the coefficient matrix is zero, as can be seen by noticing that the sum $2 \times (50) + (51) + (52)$ is identically zero. The solution can be found by writing the accompanying linear combination $2 \times (44) + (45) + (46)$ of the radical conservation equations, leading to

$$-\frac{\varepsilon}{2\alpha} \frac{d^2}{dx^2} \left(\frac{2\Lambda_{\text{O}}}{L_{\text{O}}} y_{\text{O}} + \frac{\Lambda_{\text{OH}}}{L_{\text{OH}}} y_{\text{OH}} + \frac{1}{L_{\text{H}}} y_{\text{H}} \right) = \left(\frac{k_{1f}}{\alpha k_{4f} C_{\text{M}}} - 1 \right) y_{\text{H}} - y_{\text{OH}} y_{\text{O}}.$$

From this result it is seen that near crossover the evolution of the radical pool depends on the balance between radical loss by diffusion (the terms on the left-hand side), radical production (the first term on the right-hand side), arising from departures from the crossover temperature, and radical consumption through reaction 1*b* (the second term on the right-hand side). Introducing the expansions for y_i together with (53) provides the reduced problem

$$\frac{d^2 \varphi}{d\xi^2} = \varphi(\varphi - \xi), \quad \varphi(-\infty) = \varphi(+\infty) - \xi = 0. \quad (54)$$

where the radical pool concentration

$$\varphi = \frac{\varphi_{\text{H}}^0}{[BA^2/(2\alpha)]^{1/3}} \quad (55)$$

has been introduced, along with the rescaled coordinate

$$\xi = \frac{x}{[B\varepsilon/(2\alpha A)]^{1/3}}, \quad (56)$$

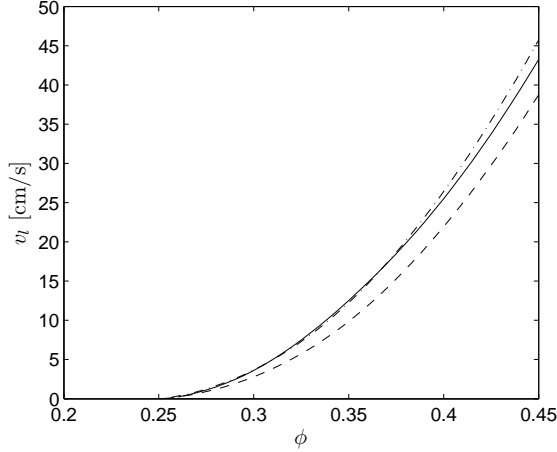


Figure 3: The variation with equivalence ratio of the planar propagation velocity of a premixed hydrogen-air flame for $p = 1$ atm and $T_u = 300$ K as obtained from the 7-step short mechanism listed in Table 1 (solid curve), from the one-step reduced mechanism (dashed curve), and from the correction with the crossover layer (dot-dashed curved).

where

$$B = \frac{2\Lambda_{\text{O}}}{L_{\text{O}}} + \frac{\Lambda_{\text{OH}}}{L_{\text{OH}}} + \frac{1}{L_{\text{H}}}. \quad (57)$$

The problem defined by (54) was first encountered by Liñán in analyzing the inner structure of diffusion flames for large Damkohler numbers [6]. It is equivalent to a problem often attributed to Friedlander and Keller [7] whose solution in the combustion context was first published by Fendell [8]; see Williams [9].

According to (17), the departures of the H-atom concentration from its steady-state value (29) result in corrections to the burning rate as dictated by the simplified form

$$\begin{aligned} \dot{m}_{\text{H}_2} - \dot{m}_{\text{H}_2,ss} \\ = 2W_{\text{H}_2}C_{\text{H}_o}\delta \int_{-\infty}^{+\infty} k_{4f}C_{\text{M}}C_{\text{O}_2}(y_{\text{H}} - y_{\text{H},ss})dx. \end{aligned} \quad (58)$$

Regarding this last equation it is clear that the errors of the steady-state approximation in the region $x \sim O(1)$, where $y_{\text{H}} - y_{\text{H},ss} \sim \varepsilon$, produces small relative errors $(\dot{m}_{\text{H}_2} - \dot{m}_{\text{H}_2,ss})/\dot{m}_{\text{H}_2} \sim \varepsilon$, whereas the departures $y_{\text{H}} - y_{\text{H},ss} \sim \varepsilon^{1/3}$ seen in the crossover layer $x \sim \varepsilon^{1/3}$ gives a much larger contribution to the burning rate, of order $(\dot{m}_{\text{H}_2} - \dot{m}_{\text{H}_2,ss})/\dot{m}_{\text{H}_2} \sim \varepsilon^{2/3}$. This last correction can be evaluated explicitly by introducing in (58) the inner variables φ and ξ to give

$$\begin{aligned} \dot{m}_{\text{H}_2} - \dot{m}_{\text{H}_2,ss} \\ = 2IW_{\text{H}_2}(k_{4f}C_{\text{M}}C_{\text{O}_2})_c C_{\text{H}_o}\delta \varepsilon^{2/3} \left(\frac{B}{2\alpha}\right)_c^{2/3} A^{1/3}, \end{aligned} \quad (59)$$

where the integral factor

$$I = \int_{-\infty}^0 \varphi d\xi + \int_0^{\infty} (\varphi - \xi) d\xi = 0.95. \quad (60)$$

accounts for the increase in radical concentration from the steady-state prediction. The extent of the resulting correction is tested in Fig.3, which compares laminar flame propagation velocities obtained with detailed chemistry with the burning-rate predictions $v_l = \dot{m}_{\text{H}_2}/(\rho_u Y_{\text{H}_2,u})$.

Conclusions and future work

An asymptotic analysis based on the relative smallness of the radical concentrations has been used to describe the burning rate of lean hydrogen-air deflagrations near the flammability limit. The results can be useful in future analyses of deflagration stability and dynamics, including curvature and strain effects.

Acknowledgements

This collaborative research was supported by the Spanish MICINN under Project # ENE2008-0615-C04 and by the Comunidad de Madrid under Project# S-505/ENE/0229. The work of DFG was supported by the Spanish MICINN through the FPU Program (AP2005-0446).

References

- [1] D. Fernández-Galisteo, A. L. Sánchez, A. Liñán, F. A. Williams, *Combust. Flame* in press (2009) (doi:10.1016/j.combustflame.2008.10.009)
- [2] Available at: <http://maemail.ucsd.edu/combustion-/cermech>.
- [3] P. Saxena, F. A. Williams, *Combust. Flame*, 145 (2006) 316–323.
- [4] Cosilab Collection, Version 2.0.7, Rotexo-Softpredict-Cosilab GmbH & Co. KG, Bad Zwischenahn (Germany), www.SoftPredict.com (2007).
- [5] J. Troe, *Proc. Combust. Inst.*, 28 (2000) 1463–1469.
- [6] A. Liñán, On the internal structure of laminar diffusion flames, OSR/EOAR, TN 62–69, INTA, Madrid (1961).
- [7] S. K. Friedlander and K.H. Keller, *Chem. Eng. Sci.* 18 (1963) 365–375.
- [8] F. E. Fendell, *J. Fluid Mech.* 21 (1965) 281–303.
- [9] F. A. Williams, *Ann. Rev. Fluid Mech.* 3 (1971) 172–174.